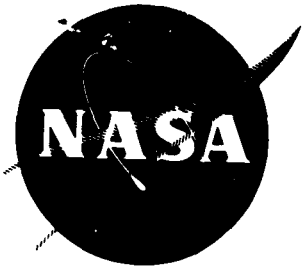

NASA CR-72246

ANALYSIS OF A GAS BEARING SYSTEM WITH SHAFT DAMPING FOR STABILITY

By

S. V. Lukas

Prepared for

NATIONAL AERONAUTICS AND SPACE ADMINISTRATION

CONTRACT NAS 3-8516

UNION CARBIDE CORPORATION

Linde Division

Tonawanda, New York

Requests for copies of this report should be referred to

National Aeronautics and Space Administration
Office of Scientific and Technical Information
Attention: AFSS-A
Washington, D.C. 20546

NASA CR-72246

FINAL REPORT

ANALYSIS OF A GAS BEARING SYSTEM WITH SHAFT DAMPING FOR STABILITY

By

S. V. Lukas

Prepared for

NATIONAL AERONAUTICS AND SPACE ADMINISTRATION

June, 1967

CONTRACT NAS 3-8516

Technical Management
NASA Lewis Research Center
Cleveland, Ohio

Space Power Systems Division
Henry B. Tryon

Fluid System Components Division
Technical Advisor - William J. Anderson

UNION CARBIDE CORPORATION

Linde Division

Tonawanda, New York

FOREWORD

This is the final report of an analytical study and design performed by Union Carbide Corporation, Linde Division, on Contract NAS3-8516. The purpose of this program is to investigate the applicability of Linde's gas bearing system to the Brayton-cycle turbomachinery, specifically the radial flow turbocompressor built under Contract NAS3-2778. The contract work was performed under the direction of National Aeronautics and Space Administration, Lewis Research Center. Mr. H. B. Tryon was the Project Manager, and Messrs. W. J. Anderson and F. J. Dutee, the Technical Advisors.

The work was conducted during the period of June 6, 1966, and January 6, 1967, by Mr. S. V. Lukas as the Principal Investigator. He was assisted by Messrs. H. H. Ammann, L. C. Kun, B. D. Patel, H. M. Scofield, and W. H. Tober.

TABLE OF CONTENTS

FIGURES

1.0 SUMMARY

This report presents the work performed for the application of Linde's gas bearing system to an existing Brayton cycle turbocompressor. After reviewing the existing turbocompressor design, the following tasks were performed:

The most suitable bearing and mount arrangement for the machine was selected. The gas-lubricated rotor is supported by a non-rotating damped shaft with flexible supports.

The journal bearings were analyzed for power loss, centrifugal and thermal growth of the radial clearances, and other pertinent performance parameters.

A spiral-grooved, pump-in thrust bearing was selected and analyzed for frictional power loss, load-carrying capacity, running gap, centrifugal and thermal distortion.

The journal bearings and the double-acting thrust bearing are provided with feeder holes of the inherently compensated type for hydrostatic start-up and stop.

The rigid body critical speeds of the system were calculated and were found to be above and below the operating speed. The flexural critical speeds of the stationary shaft and rotor were found to be above the overspeed condition of the machine.

The stiffness of the flexible supports and the required damping coefficients were determined for stable operation of the journal bearings at the design speed and overspeed.

A scale layout of the bearing and support system was made.

2.0 INTRODUCTION

NASA has presently under development a Brayton cycle space power system. Present gas bearing designs for the Brayton cycle turbomachinery are of the pivoted-pad type and may have a limited life due to wear at the pivot point. The life requirement of such bearings is 10,000 hours with no maintenance or replacement. Plain cylindrical journal bearings cannot be used because they are unstable at high speeds and in the zero "g" environment.

Figure 1 is a schematic view of the existing Brayton cycle radial flow turbocompressor using argon as the working fluid. The compressor and turbine inlet temperatures are 536°R and 1950°R, respectively, the inlet pressures are 6.0 psia and 13.2 psia, respectively, and the pressure ratios are 2.30 and 1.56, respectively. The operating speed of the machine is 38,500 rpm and has an overspeed requirement of 46,200 rpm. The journal bearings are of the pivoted-pad type and the thrust bearing of the step-sectored type. The thrust bearing stator is mounted on a gimbal so that it can follow any misalignment of the thrust runner. All bearings operate hydrodynamically in a 12-psia argon environment with hydrostatic start-up and stop.

Figure 2, attached hereto, presents the same turbocompressor utilizing Linde's gas bearing system. The system consists of a stationary shaft mounted to the inlet and outlet ducting of the turbocompressor by flexible supports. This arrangement provides thermal isolation of the bearings from the housing and, therefore, the journal bearing clearances will be affected only slightly since the shaft and rotor will follow the same temperature excursions. The thrust bearing stator, which is located near the compressor wheel, is press-fitted to the shaft forming thus an integral part with the shaft. In this arrangement, good bearing alignment is assured, and there is no need for a gimbal mount for the thrust stator. The rotor is split at the thrust bearing for assembly purposes. High-pressure argon is introduced through the compressor end flexible support for hydrostatic start-up and stop. External pressurization is shut off when the rotor reaches operating speed.

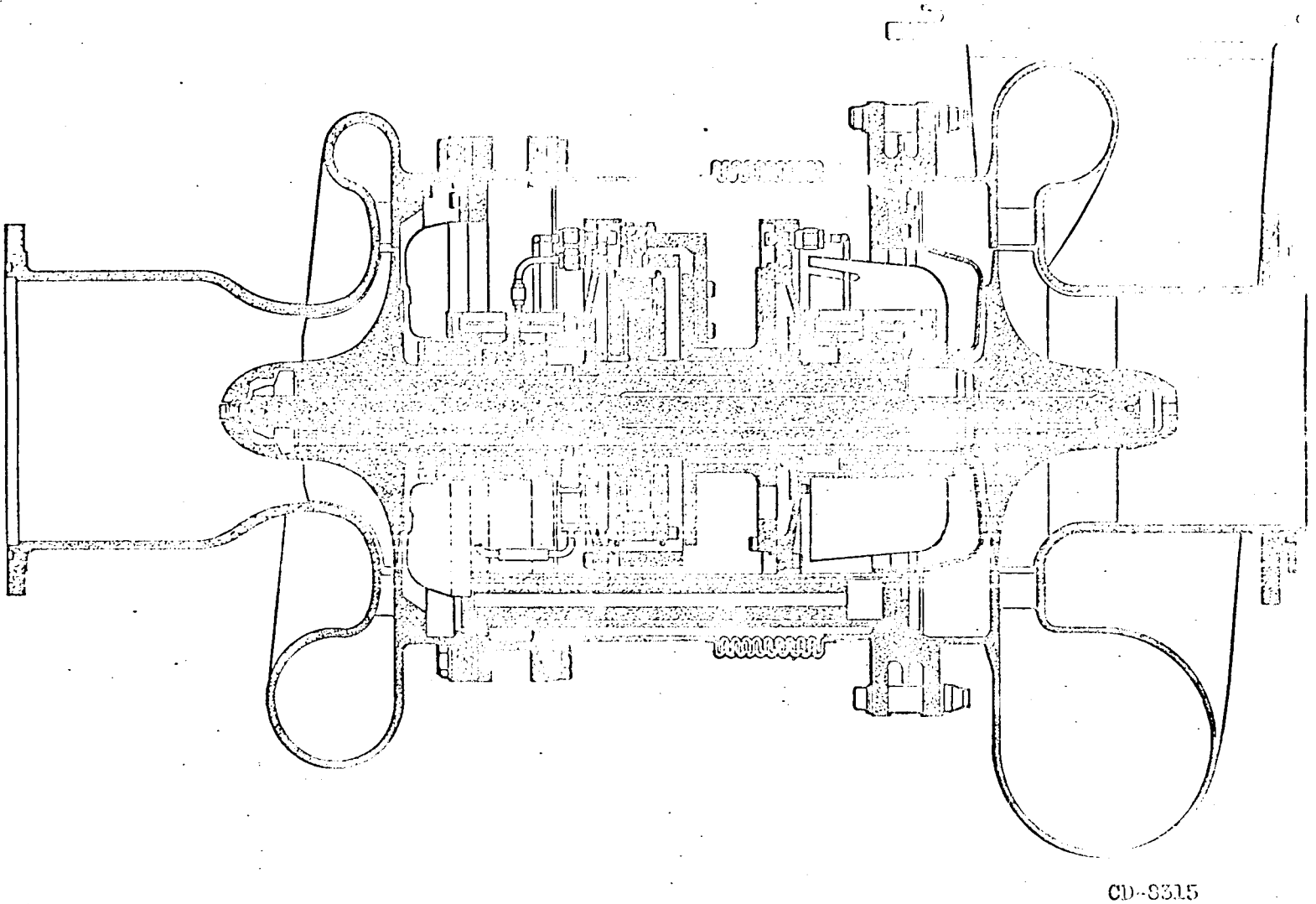

CD-8315

FIG. 1. - RADIAL TURBOCOMPRESSOR.

3.0 JOURNAL BEARING DESIGN

3.1 Journal Bearing Hydrodynamic Parameters

The machine has two full cylindrical journal bearings. Their geometrical and operating parameters under hydrodynamic conditions are given in Sections 3.1.1 and 3.1.2.

3.1.1 Geometrical Parameters

Bearing diameter:	1.33 inches
Bearing length:	1.33 inches
Radial clearance:	0.7 mil (compressor end)
	0.5 mil (turbine end)

3.1.2 Operating Parameters

	For both bearings
Speed:	38,500 rpm
Radial clearance:	1.1 mils*
Ambient pressure:	12 psia

	Compressor end bearing	Turbine end bearing
Temperature, °R:	500	1600
Viscosity, lb-sec/in^2:	3.12×10^{-9}	7.2×10^{-9}
Compressibility number:	2.30	5.30
Load, lb:	4.2	6
Eccentricity ratio:	0.28	0.25
Film stiffness, lb/inch:	17,400	25,000
Power loss, watts:	14	31

3.2 Journal Bearing Hydrostatic Parameters

Each journal bearing has a row of orifices at its center for hydrostatic start-up and stop. The geometrical and operating parameters for hydrostatic operation are given in Sections 3.2.1 and 3.2.2.

3.2.1 Geometrical Parameters

Type of restrictor:	inherently compensated
Bearing diameter:	1.33 inches
Bearing length:	1.33 inches
Radial clearance:	0.7 mil (compressor end)
	0.5 mil (turbine end)
Diameter of feeder holes:	1/32 inch
Number of feeder holes:	8 (per journal bearing)

*The radial clearances of both journal bearings increase to 1.1 mils at 38,500 rpm due to centrifugal growth. See Section 3.3.

There is some concern about loss of load-carrying capacity of the journal bearings under hydrodynamic conditions due to the back leakage through the feeder holes. The feeder holes should be located at the center of the journal bearing and away from the minimum film thickness where the pressure level is high.

3.2.2 Operating Parameters

	For both bearings
Speed:	0
Supply pressure:	84.7 psia
Ambient pressure:	12 psia
Temperature:	70 °F
Viscosity:	3.34×10^{-9} lb-sec/in^2

	Compressor end bearing	Turbine end bearing
Film stiffness, lb/inch:	49,000	39,400
Load, lb:	4.2	6
Eccentricity ratio:	0.12	0.30
Flow rate, lb/min:	0.047	0.020

3.3 Journal Bearing Centrifugal Growth

The journal bearing radial clearances will increase as the rotor speeds up due to centrifugal forces. The clearances at zero speed, design speed (38,500 rpm), and overspeed (46,200 rpm) will be as follows:

Speed rpm	Radial clearance of compressor end journal bearing mils	Radial clearance of turbine end journal bearing mils
0	0.7	0.5
38,500	1.1	1.1
46,200	1.3	1.4

A radial clearance of 1.1 mils was selected at the operating speed to provide high threshold of stability and low power loss.

The centrifugal growth, (ΔC), was calculated by assuming the rotor portion above the journal bearing region as an annular disk and then using the equation

$$\Delta C = \frac{\rho \omega^2}{4Eg} \left[(3 + \nu)\, r_i r_o^2 + (1 - \nu)\, r_i^3 \right] \qquad (1)$$

Equation (1) gives the centrifugal growth of an annular disk at the inner radius.

The values of the parameters used in equation (1) are as follows:

	Compressor end	Turbine end
Material:	Ti, 6% Al, 4% V	Inconel 713
r_i, inside radius:	0.665 inch	0.665 inch
r_o, outside radius:	1.3 inches	1.5 inches
ρ, density:	0.16 lb/in^3	0.286 lb/in^3
E, modulus of elasticity:	16 x 10^6 psi	25 x 10^6 psi
ν, Poisson's ratio:	0.33	0.29

In order to reduce the centrifugal growth, the journal bearings were located somewhat inward instead of at the extreme end of compressor and turbine wheels.

3.4 Journal Bearing Thermal Effects

In addition to the centrifugal growth of the journal bearing radial clearances, the temperature difference across a journal bearing gas film can cause changes in the radial clearance. If this temperature difference is large, it will cuase large changes in the radial clearance, and, therefore, corrective action must be taken.

Figure 3 represents the turbine end journal bearing and the stationary shaft.

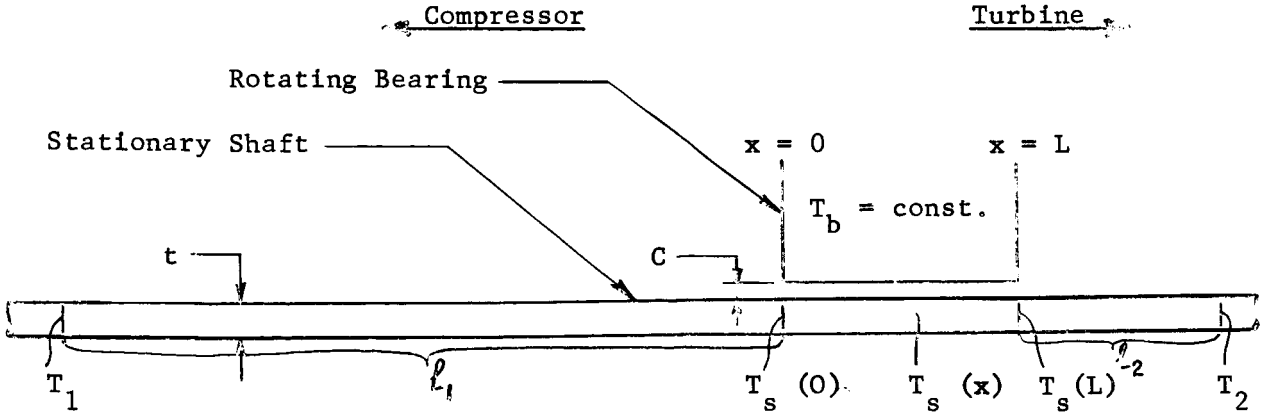

Figure 3

Journal Bearing Thermal Effects

From the energy equation with Couette flow conditions, the following expression was obtained which gives the temperature difference between the bearing and the shaft at any position x.

$$T_b - T_s(x) = \frac{1}{\sqrt{\lambda}\sinh\sqrt{\lambda}\,L}\left\{\left[\frac{dT_s(x)}{dx}\right]_0\cosh\sqrt{\lambda}\,(x-L) + \left[\frac{dT_s(x)}{dx}\right]_L\cosh\sqrt{\lambda}\,x\right\} - \frac{1}{2}\frac{\mu U^2}{Jk_g} \qquad (2)$$

where: $\lambda = \frac{k_g}{kCt}$

Setting x = 0 in equation (2), we obtain the maximum temperature difference across the gas film,

$$T_b - T_s(0) = \frac{1}{\sqrt{\lambda}\sinh\sqrt{\lambda}\,L}\left\{\left[\frac{dT_s(x)}{dx}\right]_0\cosh\sqrt{\lambda}\,L + \left[\frac{dT_s(x)}{dx}\right]_L\right\} - \frac{\mu U^2}{2Jk_g} \qquad (3)$$

where:

T_b, bearing temperature:	1632°R
$T_s(L)$, shaft temperature at x = L:	to be determined
$\left[\frac{dT_s(x)}{dx}\right]_0 \cong \frac{T_s(0) - T_1}{\ell_1}$:	$\frac{1632 - 536}{7.25} = 151.2$°F/inch
$\left[\frac{dT_s(x)}{dx}\right]_L \cong \frac{T_s(L) - T_2}{\ell_2}$:	0 (since no temperature difference was assumed toward the support)
L, bearing length:	1.33 inches
U, linear bearing velocity:	8.08×10^5 ft/hr (38,500 rpm)
C, radial clearance:	0.0011 inch
t, shaft wall thickness:	0.1 inch
k_g, gas thermal conductivity:	0.0231 Btu/hr-ft-°F (argon at 1600°R)
μ, viscosity:	2.88×10^{-10} lb-hr/ft^2 (argon at 1600°R)
k, shaft thermal conductivity:	8.5 Btu/hr-ft-°F (titanium at 1600°R)
J, Joule constant:	778 ft-lb/Btu

Substituting the above values in equation (3), we obtain

$$\lambda = \frac{0.0231}{(8.5)(0.0011)(0.1)} = 24.7/\text{sq.in.}$$

and

$$T_b - T_s(0) = \frac{1}{\sqrt{24.7}\ \sinh\ (1.33\sqrt{24.7}\ )} \left\{151.2 \cosh\ (1.33\sqrt{24.7}) + 0\right\}$$

$$- \frac{(2.88 \times 10^{-10})(8.08 \times 10^{5})^2}{(2)(778)(0.0231)}$$

$$T_b - T_s(0) = 30.4 - 5.2 = \underline{25.2°F}$$

The change in the radial clearance (ΔC) due to this temperature difference can now be calculated by the equation

$$\Delta C = \alpha R \Delta T$$

where:

α, linear expansion coefficient of Titanium (6% Al, 4% V) shaft:	6.0×10^{-6} per °F
R, journal bearing radius:	.665 in
ΔT, temperature difference:	25.2 °F

Substituting we obtain

$$\Delta C = .000100 \text{ in}$$

This is 9% of the design radial clearance (.0011 in) and therefore the effect will be small.

The approximations in the previous page

$$\left[\frac{dT_s(x)}{dx}\right]_0 \quad \text{and} \quad \left[\frac{dT_s(x)}{dx}\right]_L$$

assume linear temperature gradient in the shaft between the bearings. This implies adiabatic wall along the shaft, except at the bearings and at the end points, and constant thermal conductivity. The adiabatic wall assumption is a good one under hydrodynamic operation. Although the thermal conductivity of the shaft varies from 3.8 BTU/hr-ft-°F at 536°R to 8.5 at 1600°R, since the higher value of thermal conductivity was used the estimate is conservative.

4.0 THRUST BEARING DESIGN

4.1 Thrust Bearing Hydrodynamic Parameters

A spiral-grooved, pump-in thrust bearing was selected instead of a stepped type because it has higher load-carrying capacity and lower power loss. Both faces of the double-acting thrust bearing are grooved so that it can carry loads in both directions under hydrodynamic operation.

4.1.1 Geometrical Parameters

Outside radius:	1.75 inches
Inside groove radius:	1.35 inches
Inside radius:	0.8 inch
Total axial clearance:	6 mils
Groove depth:	2.18 mils
Number of grooves:	25
Groove angle:	17.5 degrees
Groove-to-ridge width ratio:	1.560

4.1.2 Operating Parameters

Speed:	38,500 rpm
Thurst load:	35 lb (toward the compressor)
Ambient pressure:	12 psia
Viscosity:	4×10^{-9} lb-sec/sq.in. (argon)
Temperature:	700°R
Compressibility number:	18.5
Running clearance:	0.73 mil (other side 5.27 mils)
Film stiffness:	94,000 lb/inch
Power loss:	111 watts

4.2 Thrust Bearing Hydrostatic Parameters

Since the thrust load reverses itself during transient conditions, both sides of the double-acting thrust bearing were provided with orifices so that the thrust bearing can carry loads in either direction.

4.2.1 Geometrical Parameters

Type of restrictor:	inherently compensated
Outside radius:	1.35 inch (same as inside groove radius)
Feeder hole circle, radius:	1.04 inches
Inside radius:	0.8 inch
Diameter of feeder holes:	0.0625 inch
Number of feeder holes:	15 (per side)
Total axial clearance:	6 mils

4.2.2 Operating Parameters

Speed:	0
Thrust load:	70 lb (toward the turbine)
Supply pressure:	84.7 psia
Ambient pressure:	12 psia
Viscosity:	3.34×10^{-9} lb-sec/sq.in. (argon)
Temperature:	70°F
Running clearance:	1 mil (other side, 5 mils)
Film stiffness:	79,000 lb/inch
Total flow rate:	2.5 lb/min (2.1 lb/min through 5 mils clearance and 0.4 lb/min through 1 mil clearance

4.3 Thermal Distortion of the Thrust Bearing Stator

The spiral-grooved thrust bearing can distort due to the heat generated by viscous shear in the bearing gap. Any distortion is undesirable because it reduces the load-carrying capacity. The change in the bearing gap, Δh, at the outer rim was calculated by the equation

$$\Delta h = \frac{\alpha}{k} \frac{\mu \omega^2 R_o^2 (R_o^2 + R_i^2)}{10\ Jh} \qquad (4)$$

where:

α, coefficient of linear thermal expansion:	6.4×10^{-6} per °F (beryllium)
k, coefficient of thermal conductivity:	2.014×10^{-3} Btu/sec-in-°F (beryllium)
μ, viscosity:	4×10^{-9} lb-sec/sq.in. (argon at 700°R)
ω, speed:	4032 rad/sec (36,500 rpm)
R_o, thrust bearing outside radius:	1.75 inches
R_i, thrust bearing inside radius:	0.8 inch
h, running gap:	0.00073 inch
J, Joule constant:	9336 inch-lb/Btu

Substituting the above values in equation (4), we obtain

$$\Delta h = 0.000035 \text{ inch}$$

The change in the running gap at the outer rim due to thermal distortion is 5%.

Equation (4) was obtained as follows: The heat generated due to viscous shear in the bearing gap will cause an axial temperature gradient within the stationary thrust plate. Since the outer edge of the thrust plate is free, the originally flat bearing surface will now assume a spherical curvature with radius, R, equal to

$$R = \frac{1}{\alpha} \frac{t}{\Delta T} \tag{5}$$

where t is the thickness of the thrust plate, and ΔT the temperature difference between the two faces of the thrust plate. In the analysis, it was assumed that the temperature gradient between the thrust plate faces is linear, and the temperatures at the faces are uniform.

From Fourier's one-dimensional heat conduction equation

$$\frac{t}{\Delta T} = \frac{k}{q} \tag{6}$$

and from geometrical considerations

$$R = \frac{R_o^2}{2\Delta h} \tag{7}$$

Substituting equations (6) and (7) into equation (5), we obtain

$$\Delta h = \frac{\alpha}{k} \frac{qR_o^2}{2} \tag{8}$$

where q is the heat (per unit area and per unit time) generated due to viscous shear in the bearing gap and flows axially through the thrust plate. Assuming <u>constant</u> thrust bearing gap h, the heat is equal to

$$q = \frac{\mu\omega^2(R_o^2 + R_i^2)}{2\ Jh} (.8)\ (.5) \tag{9}$$

This will yield a conservative estimate since the heat generated in a constant gap is larger than the heat generated in a distorted gap.

The factors 0.8 and 0.5 are introduced in equation (9) because the heat generated in a spiral-grooved bearing is about 80% to that of a plain bearing and about 50% of this heat flows axially.

Substituting equation (9) into equation (8), equation (4) is obtained.

4.4 Centrifugal Distortion of the Thrust Bearing Runner

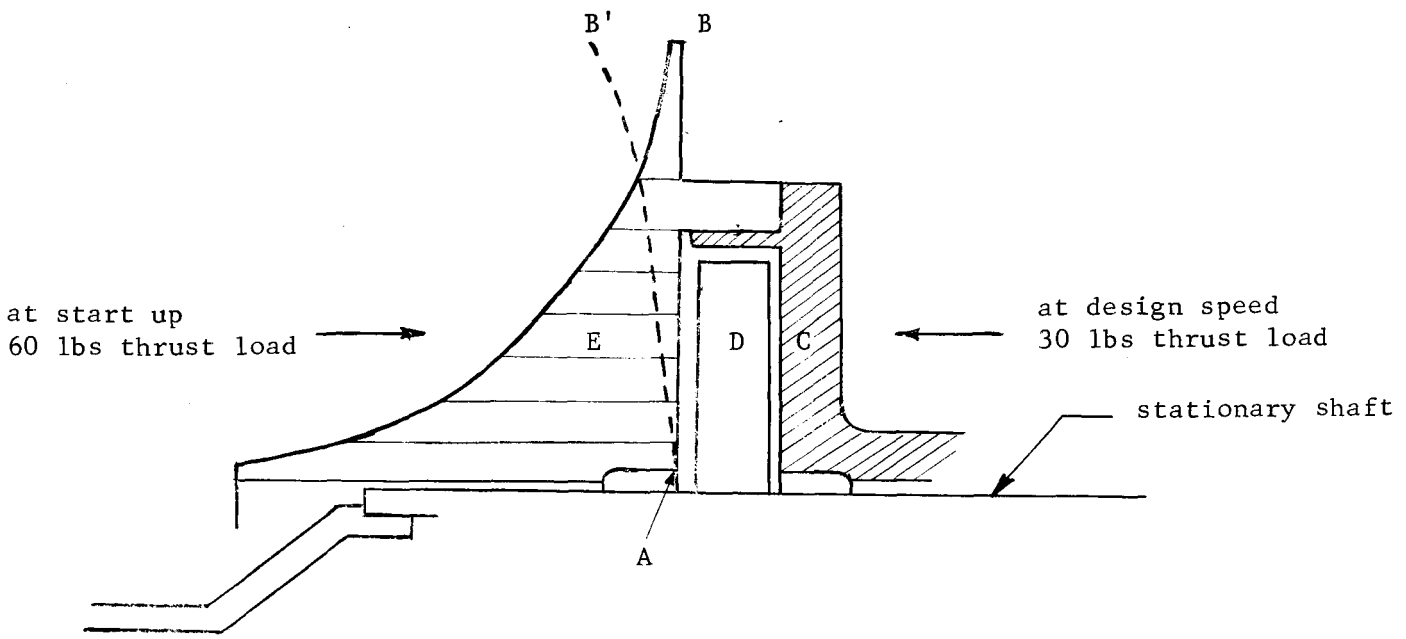

Figure 4

Bending of the Thrust Bearing Runner due to Centrifugal Forces

The thrust bearing runner which is part of the compressor wheel will deflect due to centrifugal forces. If this deflection is appreciable, it will cause loss of load-carrying capacity of the thrust bearing.

The compressor wheel and thrust bearing arrangement is shown in Figure 4. The line originally AB will assume the exaggerated position AB' under high-speed rotation. The axial deflection of the thrust surface AB as a function of radius at 46,200 rpm is shown in Figure 5. The maximum deflection at the outer rim of the thrust bearing is about 1 mil. The total axial clearance of the thrust bearing is 6 mils. The running clearance between C and D is 0.73 mil and between D and E, 5.27 mils. Therefore, a deflection of 1 mil in a 5.27-mil running clearance will not affect the thrust bearing operation.

FIGURE 5

AXIAL DEFLECTION OF THE THRUST BEARING
RUNNER VS RADIAL DISTANCE

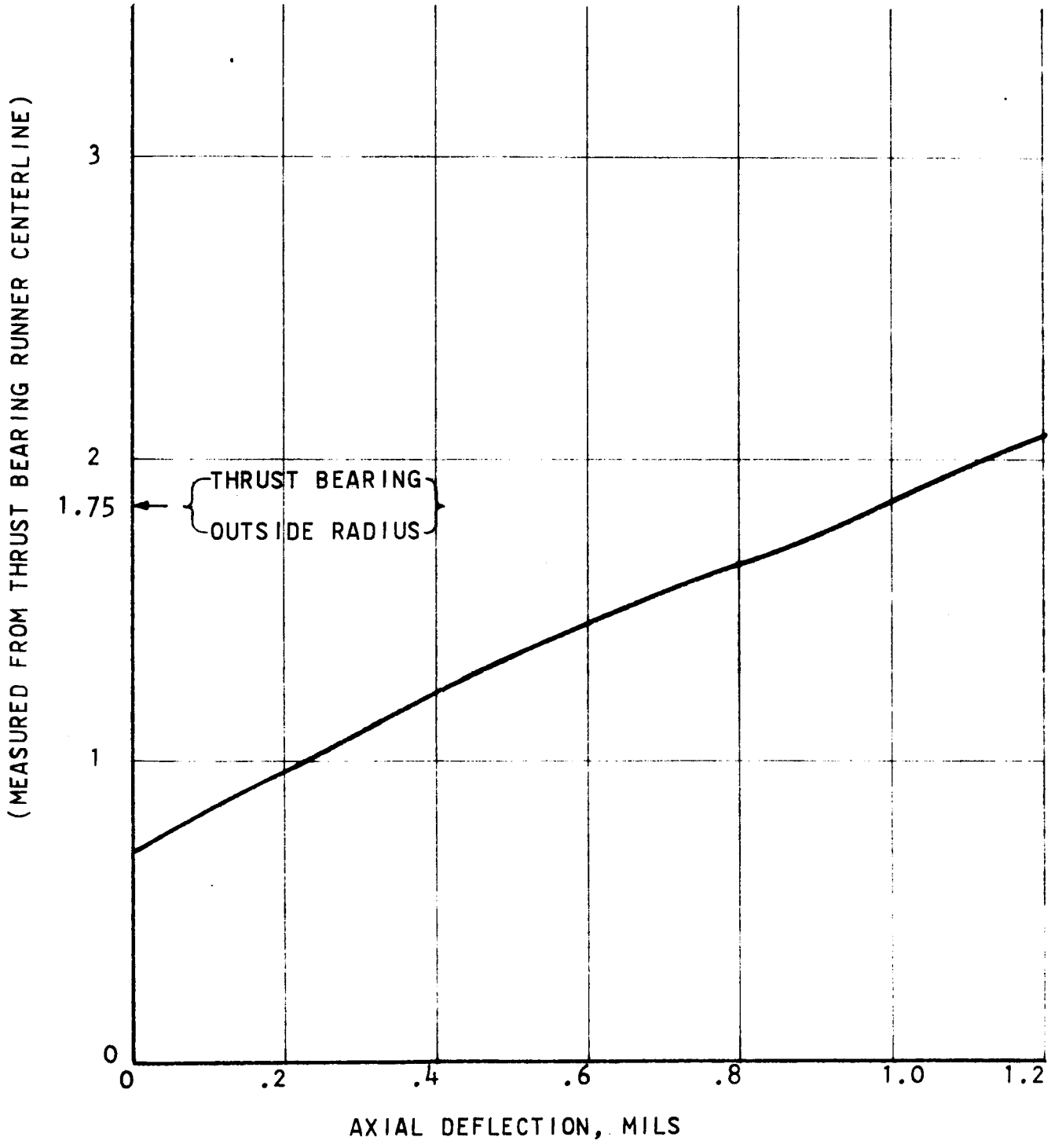

The deflection of the compressor wheel, neglecting the blades, was found according to the method described by Roark (Ref. 4) as follows: The compressor wheel was divided into eight concentric rings. Each ring is acted on by normal stresses, body forces, and unknown moments. Equating the slopes of adjacent rings, seven equations were obtained in terms of the seven unknown moments. Having found the moments, the deflections of each ring were calculated. The deflections were then added to find the total deflection of the wheel.

In reality since the counterbalancing and stiffening effect of the blades was neglected in this analysis, the predicted deflection is much larger than what is actually anticipated.

Although member C will tend to reduce the deflection of member E, the connection was designed as a shear compliance joint with the intent to minimize any interaction between faces E and C.

5.0 BEARING-ROTOR DYNAMICS

5.1 Rigid Body Critical Speeds

The rigid body critical speeds of the gas bearing system (shaft, rotor, flexible supports, and gas film) can be determined from the equivalent mechanical system shown in Figure 6.

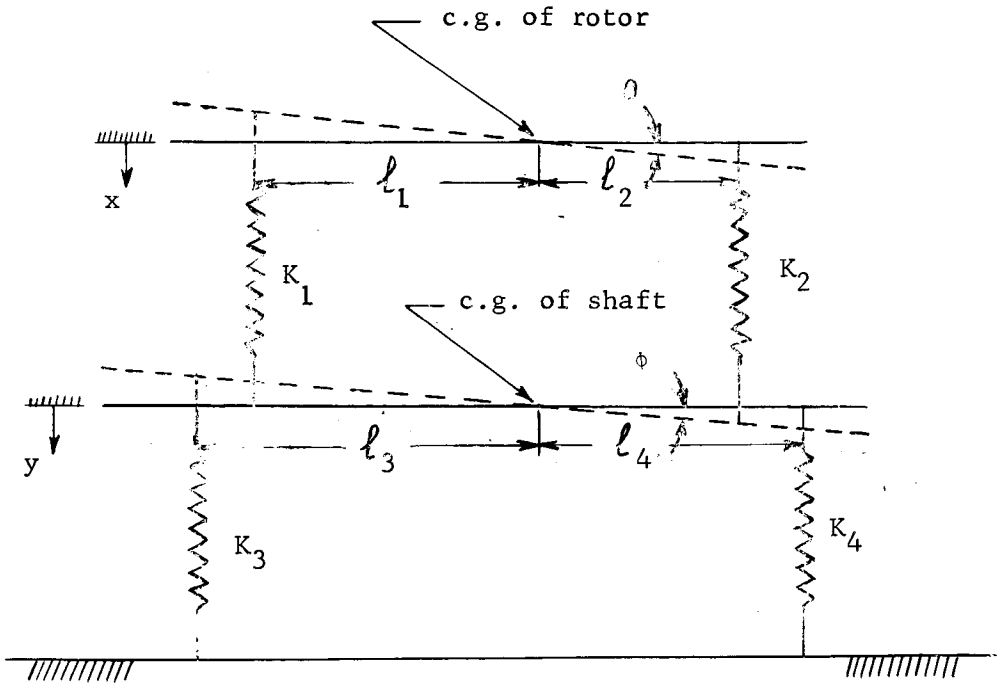

Figure 6

Vibrational Model of the Gas Bearing System

The vibrations of the two-degree-of-freedom system shown in Figure 6 are uncoupled; that is, the system has two translational and two angular critical frequencies which are independent of each other. For the vibrations to be uncoupled, the following conditions must be satisfied.

1) The center of gravity of the shaft and rotor must coincide.

2) $K_1 \ell_1 = K_2 \ell_2$

3) $K_3 \ell_3 = K_4 \ell_4$

The equations of motion of the system are:

For translation:

$$\left.\begin{aligned} M_r \ddot{x} + (K_1 + K_2)x - (K_1 + K_2)y &= 0 \\ M_s \ddot{y} + (K_1 + K_2 + K_3 + K_4)y - (K_1 + K_2)x &= 0 \end{aligned}\right\} \tag{10}$$

For rotation:

$$\left.\begin{aligned} I_r \ddot{\theta} + (K_1\ell_1^2 + K_2\ell_2^2)\theta - (K_1\ell_1^2 + K_2\ell_2^2)\phi &= 0 \\ I_s \ddot{\phi} + (K_1\ell_1^2 + K_2\ell_2^2 + K_3\ell_3^2 + K_4\ell_4^2)\phi - (K_1\ell_1^2 + K_2\ell_2^2)\theta &= 0 \end{aligned}\right\} \tag{11}$$

The lower and higher critical frequencies of the system were obtained from the following equation:

$$\omega = \left[\frac{A}{2} \pm \frac{1}{2} \sqrt{A^2 - 4B} \right]^{1/2} \tag{12}$$

where:

For translation:

$$A = \frac{M_r(K_1 + K_2 + K_3 + K_4) + M_s(K_1 + K_2)}{M_r M_s}$$

$$B = \frac{(K_1 + K_2)(K_3 + K_4)}{M_r M_s}$$

For rotation:

$$A = \frac{I_r(K_1\ell_1^2 + K_2\ell_2^2 + K_3\ell_3^2 + K_4\ell_4^2) + I_s(K_1\ell_1^2 + K_2\ell_2^2)}{I_r I_s}$$

$$B = \frac{(K_1\ell_1^2 + K_2\ell_2^2)(K_3\ell_3^2 + K_4\ell_4^2)}{I_r I_s}$$

The numerical values of the parameters which were substituted in equation (12) to obtain the critical speeds are as follows:

M_r, mass of the rotor:	0.0264 lb-sec^2/inch
M_s, mass of the shaft:	0.0033 lb-sec^2/inch
I_r, transverse moment of inertia of the rotor:	0.3940 lb-sec^2-inch
I_s, transverse moment of inertia of the shaft:	0.0493 lb-sec^2-inch
K_3, flexible support stiffness (compressor end):	8300 lb/inch
K_4, flexible support stiffness (turbine end):	9500 lb/inch
ℓ_1 (see Figure 6):	5.0 inches
ℓ_2 (see Figure 6):	3.5 inches
ℓ_3 (see Figure 6):	6.1 inches
ℓ_4 (see Figure 6):	5.4 inches

The journal bearing film stiffness K and film damping B are functions of the compressibility number Λ and eccentricity ratio ϵ. Table I shows the film stiffness and film damping for three radial clearances, 1.0, 1.1 (design clearance), and 1.2 mils at 38,500 rpm and Table II at 46,200 rpm.

Table I *

at 38,500 rpm

C mils	Λ_1	Λ_2	ϵ_1	ϵ_2	K_1 lb/inch	K_2 lb/inch	B_1 lb-sec/inch	B_2 lb-sec/inch
1.0	2.78	6.42	0.25	0.24	21,200	28,700	3.49	2.26
1.1	2.30	5.30	0.28	0.25	17,400	25,000	3.47	2.27
1.2	1.93	4.46	0.30	0.26	13,300	22,100	3.25	2.30

* Subscript 1 refers to the compressor end bearing and 2 to the turbine end bearing.

Table II

at 46,200 rpm

C mils	Λ_1	Λ_2	ϵ_1	ϵ_2	K_1 lb/inch	K_2 lb/inch	B_1 lb-sec/inch	B_2 lb-sec/inch
1.0	3.34	7.70	0.22	0.23	23,400	29,700	2.70	1.76
1.1	2.76	6.37	0.25	0.24	19,300	26,100	2.59	1.70
1.2	2.32	5.35	0.28	0.25	15,900	23,000	2.63	1.68

The lower and higher translational frequencies, and the lower and higher angular frequencies based on film stiffness at 38,500 and 46,200 rpm are shown in Tables III and IV.

Table III

Based on film stiffness at 38,500 rpm

Radial clearance mils	Rigid body critical speeds, rpm			
	Translational		Angular	
	Lower	Higher	Lower	Higher
1.0	6,513	44,732	8,824	53,365
1.1	6,379	42,068	8,538	50,596
1.2	6,227	39,422	8,165	47,731

Table IV

Based on film stiffness at 46,200 rpm

Radial clearance mils	Rigid body critical speeds, rpm			
	Translational		Angular	
	Lower	Higher	Lower	Higher
1.0	6,551	45,821	8,939	54,645
1.1	6,437	43,156	8,671	51,818
1.2	6,303	40,759	8,375	49,335

5.2 Journal Bearing Stability

The journal bearing stability maps for the translational and angular modes at 1.1 mils radial clearance are shown in Figures 7 and 8. The curves show the required amount of damping in the shaft to ensure stability at a given speed. The region under the curve is unstable and above the curve stable. Although the threshold of instability has not been determined, it should be above 70,000 rpm. Additional shaft damping values for 1.0 and 1.2 mils radial clearance, based on film properties at 38,500 rpm and 46,200 rpm, are shown in Tables V and VI. As it can be seen from Tables V and VI the smaller clearances require less shaft damping than the larger clearances. This is because the film stiffness decreases as the radial clearance increases.

Table V

Based on film stiffness and film damping at 38,500 rpm

Radial clearance mils	Shaft damping, lb-sec/inch	
	Translational	Angular
1.0	1.395	1.518
1.1	1.962	2.281
1.2	2.720	3.565

Table VI

Based on film stiffness and film damping at 46,200 rpm

Radial clearance mils	Shaft damping, lb-sec/inch	
	Translational	Angular
1.0	1.231	1.365
1.1	1.652	1.928
1.2	2.324	2.862

The damping is provided by inserting a tube in the shaft, as shown in Figure 2, which is filled to one-half of its volume with copper pellets of 0.1 mil diameter. The atmosphere within the tube is argon. Under these conditions the shaft damping will be 3.4 lb -sec/in at 38,500 rpm and 4.1 lb -sec/in at 46,200 rpm. As it can be seen from Tables V and VI, the available shaft damping is greater than the required damping for stability, with the exception of 1.2 mil radial clearance. Therefore, care must be taken not to exceed the 1.1 mil radial clearance at design speed.

FIGURE 7

STABILITY MAP-TRANSLATIONAL MODE
SHAFT DAMPING VS SPEED

RADIAL CLEARANCE: 1.1 MILS

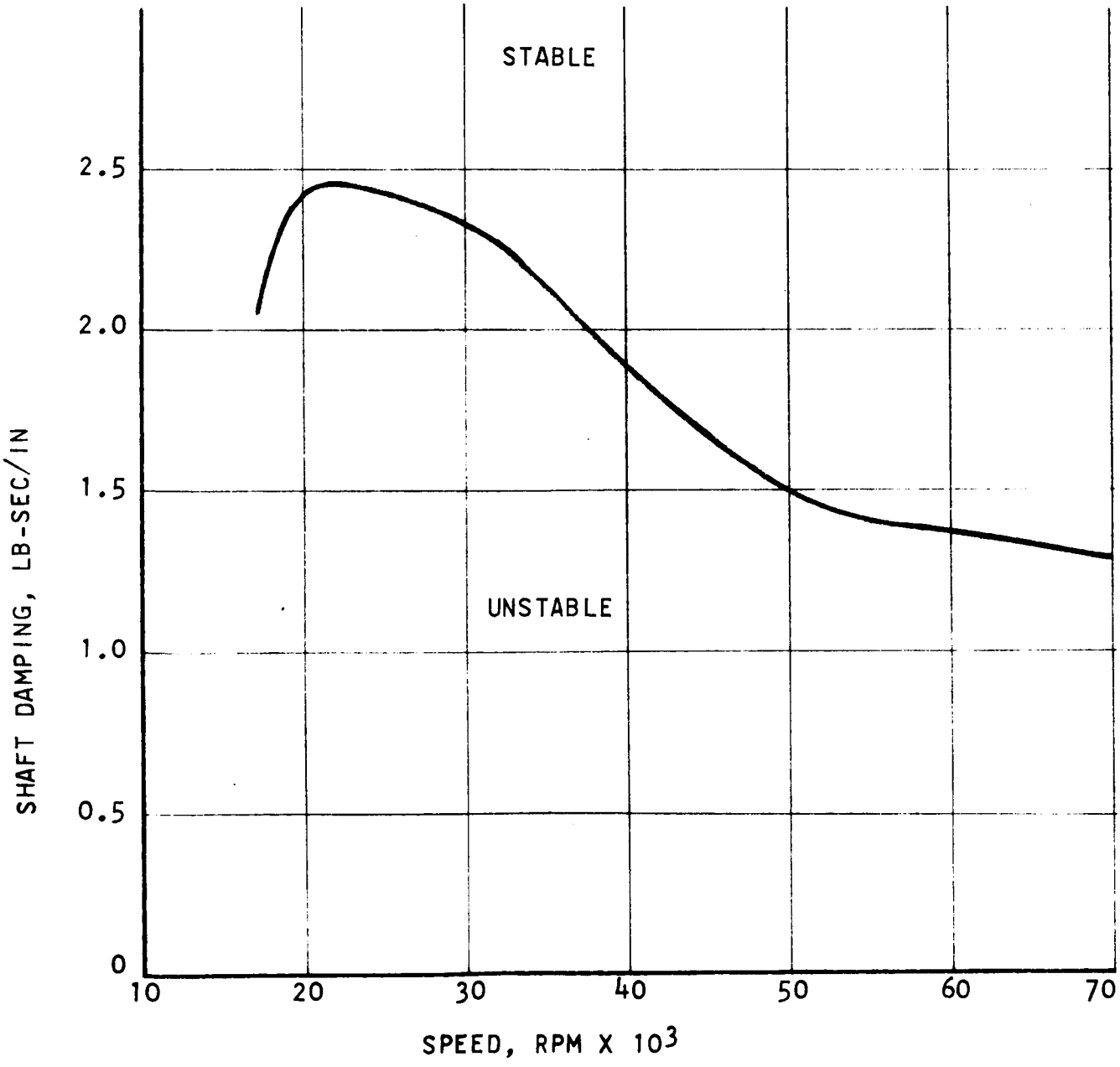

FIGURE 8

STABILITY MAP-ANGULAR MODE
SHAFT DAMPING VS SPEED

RADIAL CLEARANCE: 1.1 MILS

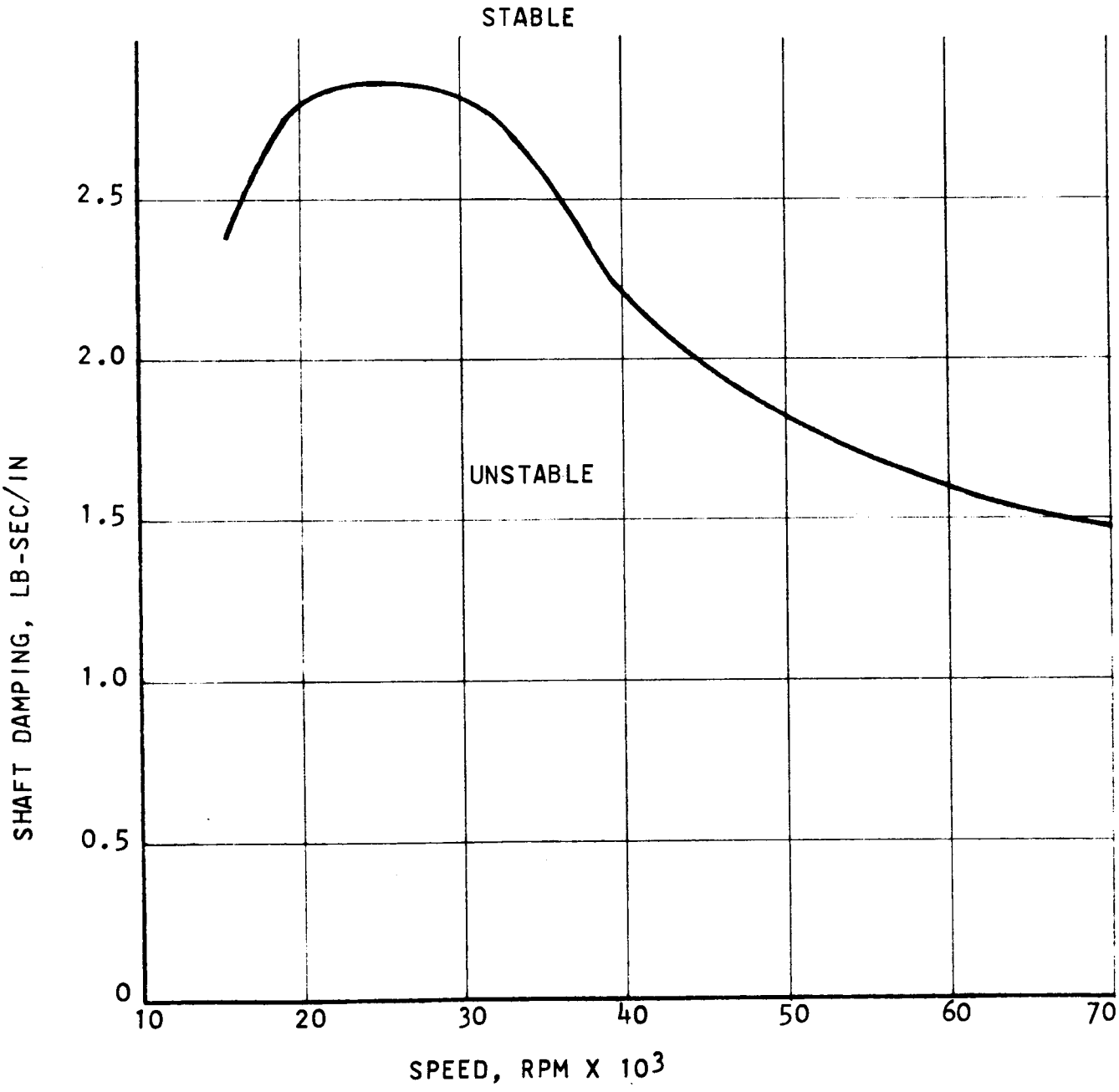

6.0 FLEXURAL CRITICAL SPEEDS

6.1 Flexural Critical of Stationary Shaft

The fundamental flexural critical speed of the shaft was determined by assuming the shaft as a clamped-clamped beam with uniformly distributed load. The length of the beam was taken to be equal to that of the shaft and the flexible supports. This method should give a conservative answer; since the stiffness of the flexible supports is much lower than that of the shaft, the shaft will vibrate as a free-free beam and, therefore, will have a higher flexural critical speed. The fundamental mode of a uniformly loaded, clamped-clamped beam is given by the equation

$$\omega = \frac{22.4}{\ell^2}\sqrt{\frac{EIg}{\rho A}} \qquad (13)$$

where:

ω, fundamental frequency:	to be determined, rad/sec
ℓ, length:	15.5 inches (shaft and flexible supports)
E, modulus of elasticity (dynamic):	10.5×10^6 psi (Ti, 6% Al, 4% V, at 1200°F)
ρ, density:	0.160 lb/cu.in.
A, cross-sectional area:	$\frac{\pi}{4}(1.33^2 - 1.13^2) = 0.3864$ sq.in.
I, moment of inertia:	$\frac{\pi}{64}(1.33^4 - 1.13^4) = 0.0736$ in.^{4}
g, dimensional constant:	386.09 inch-lb_m/lb_f-sec^2

Substituting the above values in equation (13), we obtain:

$$\omega = 6{,}477 \text{ rad/sec} = 61{,}857 \text{ rpm}$$

which is above the overspeed condition.

6.2 Flexural Critical of Rotor

The rotor shown in Figure 2 being annular will have a flexural critical speed higher than that of the existing turbocompressor (55,000 rpm) shown in Figure 1.

7.0 BEARING SYSTEM MATERIALS AND THERMAL COMPATIBILITY

The materials for the compressor and turbine wheels are titanium (6% Al, 4% V) and Inconel 713 respectively. The stationary shaft material is Titanium (6% Al, 4% V) and that of the flexible supports Inconel X-750. The reason for selecting Titanium as the shaft material is to make the mass of the shaft small in comparison to the mass of the rotor. In general, the smaller the mass of the shaft is the higher the whirl threshold will be. Inconel 713 shaft could be used with a smaller wall thickness (about 1/16 inches) than that of Titanium shaft (.100 in) so that to keep the mass the same. This material selection may be more compatible thermally. The turbine and compressor end journal bearing bushings are of the same material as that of the wheels, i.e. Inconel 713 and Titanium. All mating bearing surfaces are flame sprayed with chrome oxide coating to a 3 mil thickness.

The thrust plate stator material is Beryllium (density = .07 lb/in^3) and therefore adds little to the mass of the shaft. In addition, Beryllium has low coefficient of thermal expansion-to-thermal conductivity ratio in comparison to other materials which reduces the distortion of the thrust plate due to viscous shear.

The bearing material thermal compatibility problem should be further investigated if this bearing system is to be used in the radial flow turbocompressor. This can be done after the analytical studies of this contract pertaining to journal bearing stability have been experimentally verified.

The problem of differential thermal expansion between housing and rotor is of concern for any turboexpander. To avoid difficulty care must be taken to match the thermal expansion of rotor and housing. Similar designs have run successfully at cyrogenic temperatures with a ΔT of over 400°F and with rotor-to-shroud clearance 10 mils at ambient temperature.

8.0 CONCLUSIONS

The analytical work performed under this contract showed that full cylindrical journal bearings with flexible damped supports used in conjunction with a stationary shaft can meet the requirements of this contract, i.e., high threshold of stability, low bearing power loss, long bearing life, and thermal isolation of bearing and support from the housing. In addition, it is apparent that this arrangement will provide a simple design, easy alignment, and reduced weight.

9.0 RECOMMENDATIONS

Since the results of this analysis were encouraging, it is recommended that the following additional work be done:

1) investigate the effect of feeder holes on hydrodynamic operation

2) build a gas bearing tester to verify experimentally the analytical findings.

NOMENCLATURE

Λ	compressibility number, $\frac{6\mu\omega}{p_a}\left(\frac{R}{C}\right)^2$
μ	viscosity, lb-sec/in^2 or lb-hr/ft^2
C	journal bearing radial clearance, in. or mils
R	journal bearing radius, in.
p_a	ambient pressure, psia
ω	speed or critical frequency, rad/sec.
ΔC	centrifugal growth of journal bearing radial clearance, in.
ρ	density, lb/in^3
E	modulus of elasticity, psi
r_o	outside radius (annular disk), in.
r_i	inside radius (annular disk), in.
ν	Poisson's ratio
T_b	bearing temperature, °F
T_s	shaft temperature, °F
U	linear bearing velocity, ft/hr
L	bearing length, in.
k_g	gas thermal conductivity, Btu/hr-ft-°F
k^g	coefficient of thermal conductivity (shaft or thrust plate), Btu/hr-ft-°F or Btu/sec-in.-°F
h	thrust bearing running gap, in.
Δh	change of thrust bearing gap, in.
R_o	thrust bearing outside radius, in.
R_i	thrust bearing inside radius, in.
α	coefficient of linear thermal expansion, per °F
t	shaft wall or thrust plate thickness, in.
q	heat, Btu/in.^{2}-sec
ΔT	temperature difference, °F
M_r	mass of the rotor, lb-sec^2/in.
M_s	mass of the shaft, lb-sec^2/in.
I_r	transverse moment of inertia of the rotor, lb-sec^2-in.
I_s	transverse moment of inertia of the shaft, lb-sec^2-in.
K_1, K_2	journal bearing film stiffness (compressor end and turbine end), lb/in.
K_3, K_4	flexible support stiffness (compressor end and turbine end), lb/in.
B_1, B_2	journal bearing film damping (compressor end and turbine end), lb-sec/in.
ϵ_1, ϵ_2	eccentricity ratio (compressor end and turbine end)
x, y	translation of the center of gravity of rotor and shaft, in.
θ, ϕ	rotation of the center of gravity of rotor and shaft, rad.
I	moment of inertia of area, in.^{4}
A	cross-sectional area, in.^{2}
J	Joule constant, 778 ft-lb/Btu or 9336 in-lb/Btu
g	dimensional constant, 386.09 in-lb$_m$/lb$_f$-sec^2

REFERENCES

1. "Design of Gas Bearings," Mechanical Technology, Inc., Latham, New York, June 1966, Vol. I, Sections: 5.3, 5.5, 6.1, 6.3, and 8.1; Vol. II, Section: 12.4.

2. "Gas Lubricated Bearings," edited by Grassam, N. D., and Powell, J. W., Butterworths, London, 1964, Sections: 2.7 and 2.11.

3. Pan, C. H. T., and Sternlicht, B., "Distortion of Gas Thrust Bearing due to Viscous Shear," Report No. MTI-65TR49, Mechanical Technology, Inc., Latham, New York, December 1965.

4. Roark, R. J., "Formulas for Stress and Strain," McGraw-Hill, New York, N. Y., 4th edition, 1965, pp. 250, 308.

ANALYSIS OF A GAS BEARING SYSTEM WITH SHAFT DAMPING FOR STABILITY

by

S. V. Lukas

ABSTRACT

The application of Linde's gas bearing system to Brayton-cycle turbomachinery was investigated. The bearing arrangement was selected for the radial flow turbocompressor built under Contract NAS 3-2778. The stiffness of the flexible supports and the shaft damping were determined to ensure journal bearing stability. Also, all other pertinent bearing parameters were determined.

REPORT DISTRIBUTION LIST FOR
CONTRACT No. NAS3-8516

NASA Lewis Research Center
21000 Brookpark Road
Cleveland, Ohio 44135

Attention: H. B. Tryon (3)
Mail Stop 500-201

W. J. Anderson (1)
Mail Stop 23-2

D. G. Beremand (1)
Mail Stop 500-201

D. T. Bernatowicz (1)
Mail Stop 500-201

R. L. Cummings (1)
Mail Stop 3-15

J. H. Dunn (1)
Mail Stop 500-201

F. J. Dutee (1)
Mail Stop 21-4

J. A. Heller (1)
Mail Stop 500-201

B. Lubarsky (1)
Mail Stop 500-201

T. A. Moss (1)
Mail Stop 500-201

Z. N. Nemeth (1)
Mail Stop 6-1

J. E. Dilley (1)
Mail Stop 500-309

P. E. Foster (1)
Mail Stop 3-19

N. T. Musial (1)
Mail Stop 501-3

Library (2)
Mail Stop 60-3

Report Control Office (1)
Mail Stop 5-5

NASA Scientific and Technical Information Facility
Post Office Box 33 (1 + Reproducible)
College Park, Maryland 20740
Attn: Acquisitions Branch (SQT-34054)

National Aeronautics and Space Administration
Washington, D. C. 20546

Attention: Herbert D. Rochen (1)
Code RNP

RNP/Dr. Fred Schulman (1)

RNW/Arvin Smith (1)

NASA/LeRC Resident Management Office
Pratt & Whitney Aircraft (1)
Florida Research and Development Center
West Palm Beach, Florida 33402
Attention: G. K. Fischer

NASA Ames Research Center (1)
Moffett Field, California 94035
Attention: Library

NASA Flight Research Center (1)
Post Office Box 273
Edwards, California 93523
Attention: Library

NASA Goddard Space Flight Center
Greenbelt, Maryland 20771
Attention: Library

NASA Langley Research Center
Langley Station
Hampton, Virginia 23365
Attention: Library

NASA Manned Spacecraft Center
Houston, Texas 77058
Attention: Library

NASA Manned Spacecraft Center
Houston, Texas 77058
Attention: Tony Redding

NASA Marshall Space Flight Center
Huntsville, Alabama 35812
Attention: Library

NASA Western Operations Office
150 Pico Boulevard
Santa Monica, California 90406
Attention: Library

Jet Propulsion Laboratory
4800 Oak Grove Drive
Pasadena, California 91103
Attention: Library

Wright-Patterson Air Force Base,
Ohio 45433
Attention: George Thompson
(APFL, Air Force Aero Propulsion)

U. S. Army Engineer R&D Labs.
Gas Turbine Test Facility
Fort Belvoir, Virginia 22060
Attention: W. Crim

Office of Naval Research
Department of the Navy
Washington, D. C. 20025
Attention: Dr. Ralph Roberts

Bureau of Ships
Department of the Navy
Washington, D. C. 20025
Attention: G. L. Graves

Bureau of Naval Weapons
Department of the Navy
Washington, D. C. 20025
Attention: Code RAPP

Air Force Systems Command
Aeronautical Systems Division
Wright-Patterson Air Force
Base, Ohio 45433
Attention: Librarian

Institute for Defense Analyses
400 Army-Navy Drive
Arlington, Virginia 22202
Attention: Librarian

Power Information Center
University of Pennsylvania
Room 2107
3401 Market Street
Philadelphia, Pennsylvania 19104

Aerojet-General Corporation
Azusa, California 91703
Attention: Librarian

AiResearch Mfg. Company
The Garrett Corporation
402 South 36 Street
Phoenix, Arizona 85034
Attention: Librarian

AiResearch Mfg. Company
The Garrett Corporation
402 South 36 Street
Phoenix, Arizona
Attention: E. L. Wheeler

AiResearch Mfg. Company
The Garrett Corporation
9851 Sepulveda Boulevard
Los Angeles, California 90009
Attention: Librarian

Bendix Research Labs. Division
Southfield (Detroit), Michigan 48232
Attention: Librarian

The Boeing Company
Aero-Space Division
Box 3707
Seattle, Washington 98124
Attention: Librarian

Borg-Warner Corporation
Pesco Products Division
24700 North Miles Road
Bedford, Ohio 44014
Attention: Librarian

Continental Aviation & Engineering
Corporation
12700 Kercheval Avenue
Detroit, Michigan 48215
Attention: Librarian

Curtiss-Wright Corporation
Wright Aero Division
Main & Passaic Streets
Woodridge, New Jersey 07075
Attention: Librarian

Douglas Aircraft Company
3000 Ocean Park Boulevard
Santa Monica, California 90406
Attention: Librarian

Franklin Institute Laboratories
Benjamin Franklin Parkway at 20th St.
Philadelphia, Pennsylvania 19103
Attention: Otto Decker

General Dynamics Corporation
16501 Brookpark Road
Cleveland, Ohio 44142
Attention: Librarian

General Electric Company
FPLD
Cincinnati, Ohio 45215
Attention: Librarian

General Electric Company
Mechanical Technology Laboratory
R&D Center
Schenectady, New York 12301
Attention: Librarian

General Electric Company
Missile and Space Division
Cincinnati, Ohio 45215
Attention: M. A. Zipkin

General Electric Company
Missile & Space Vehicle Department
3198 Chestnut Street
Philadelphia, Pennsylvania 19104
Attention: Librarian

General Motors Corporation
Indianapolis, Indiana 46206
Attention: Librarian

Lear Siegler, Inc.
3171 S. Bundy Drive
Santa Monica, California 90406
Attention: Librarian

Lockheed Missiles & Space Company
P.O. Box 504
Sunnyvale, California 94088
Attention: Librarian

Massachusetts Institute of
Technology
Cambridge, Massachusetts 02139
Attention: Librarian

Mechanical Technology Inc.
968 Albany-Shaker Road
Latham, New York 12110
Attention: Librarian

P. Curwen

North American Aviation, Inc.
Space and Information Systems Div.
Downey, California 90241
Attention: Librarian

Northern Research & Engineering Co.
219 Vassar Street
Cambridge, Massachusetts 02139
Attention: Librarian

Pratt & Whitney Aircraft
400 Main Street
East Hartford, Connecticut 06108
Attention: Librarian

Peter Bolan, APS-2J (1)

Ronald Cohen, APS-2J (1)

Solar, Div. of International Harvester
2200 Pacific Highway
San Diego, California 92112
Attention: Librarian

Space Technology Laboratories, Inc.
One Space Park
Redondo Beach, California 90278
Attention: Librarian

Sunstrand Denver
2480 West 70 Avenue
Denver, Colorado 80221
Attention: Librarian

TRW Accessories Division
23555 Euclid Avenue
Cleveland, Ohio 44117
Attention: Librarian

United Aircraft Research Laboratory
East Hartford, Connecticut 06108
Attention: Librarian

University of Maryland
College of Engineering
College Park, Maryland 20740
Attention: M. E. Talaat

University of Virginia
School of Engineering & Applied
Science
Department of Mechanical Engineering
Charlottesville, Virginia 22903
Attention: Dr. E. Gunter, Jr.

Westinghouse Electric Corporation
Astronuclear Laboratory
P.O. Box 10864
Pittsburgh, Pennsylvania 15236
Attention: Librarian

Williams Research
Walled Lake, Michigan 48088
Attention: Librarian